atmosphere

MDPI

Type of the Paper (Article)

Damaging convective and non-convective winds in southwestern Iberia during Windstorm Xola

Paulo Pinto [1,†], and Margarida Belo-Pereira [1,2,†,*]

1 Meteorology and Geophysics Department, Portuguese Institute for Sea and Atmosphere (IPMA), Portugal
2 Center for the Research and Technology of Agro-Environmental and Biological Sciences (CITAB), University of Trás-os-Montes and Alto Douro, 5001-801 Vila Real, Portugal
† These authors contributed equally to this work.
* Correspondence: IPMA, Rua C ao Aeroporto, 1749-077 Lisboa, margarida.belo@ipma.pt

Received: 30 May 2020; Accepted: 26 June 2020, Published: 30 June 2020

Supplementary Material

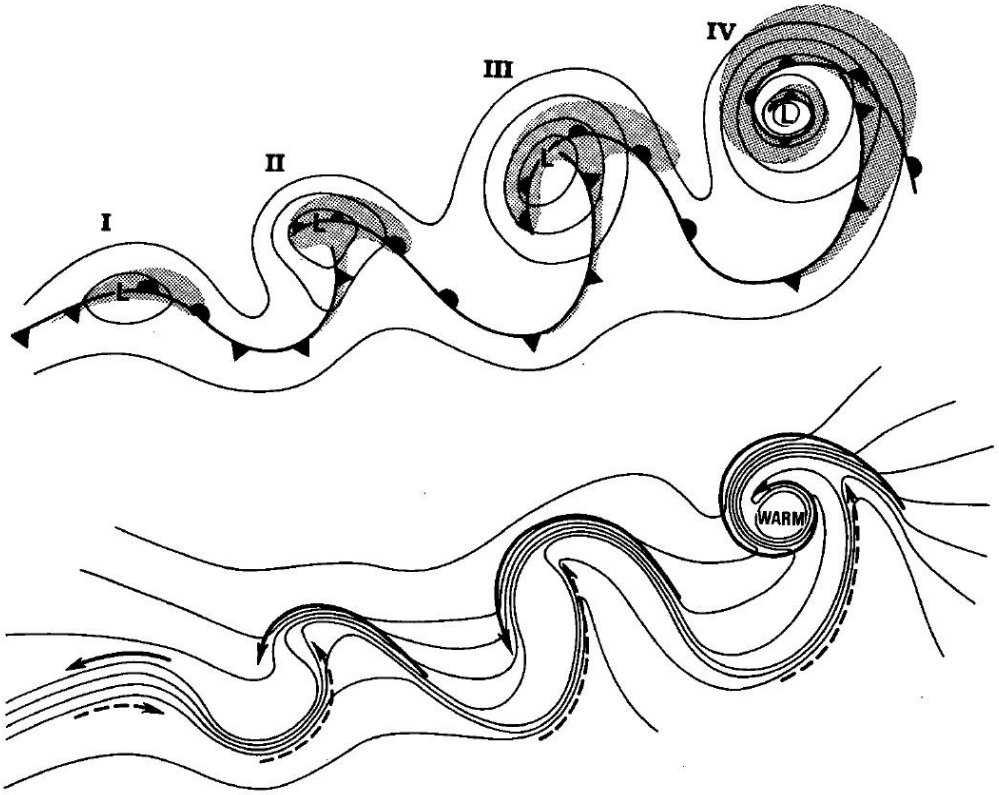

Figure S1. Shapiro-Keyser conceptual model: incipient frontal cyclone (I); frontal fracture (II), frontal T bone and bent-back front (III) and warm-core seclusion (IV). From Shapiro and Keyser [1]. Upper: Mean sea level pressure (solid), fronts (bold) and cloud signature (shaded). Bottom: temperature (solid) and cold and warm air (solid and dashed arrows, respectively).

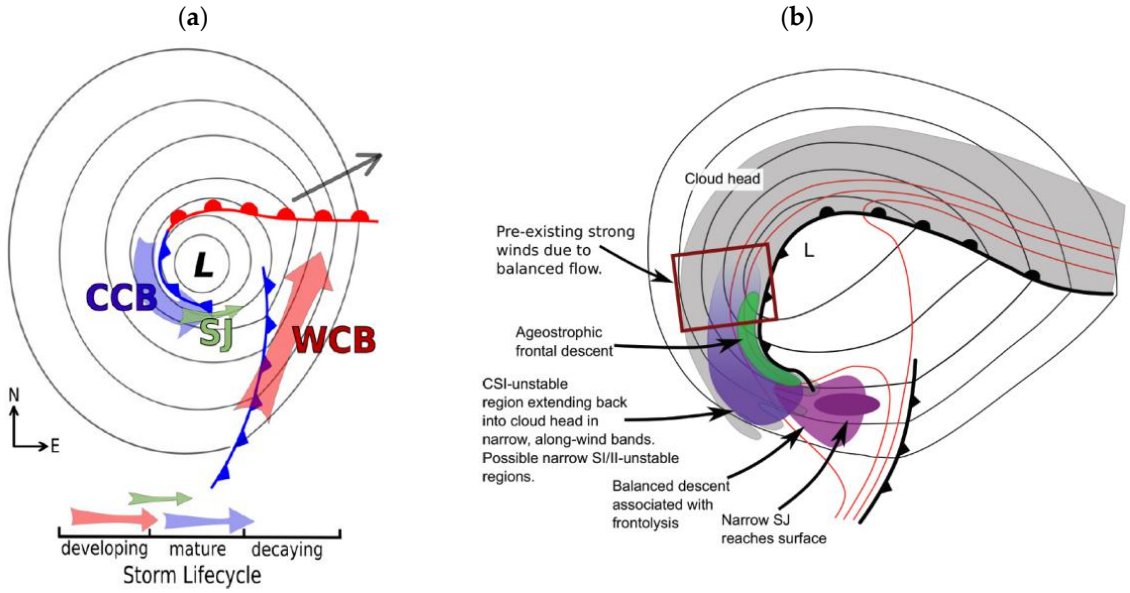

Figure S2. Conceptual model of sting jet: **(a)** Model presented by Hart *et al.* [20], showing the cold front, the bent-back front, the Cold Conveyor Belt (CCB), Warm Conveyor Belt (WCB) and the sting jet (SJ). **(b)** Model presented by Clark and Gray [14], explaining the mechanisms involved in the sting jet formation.

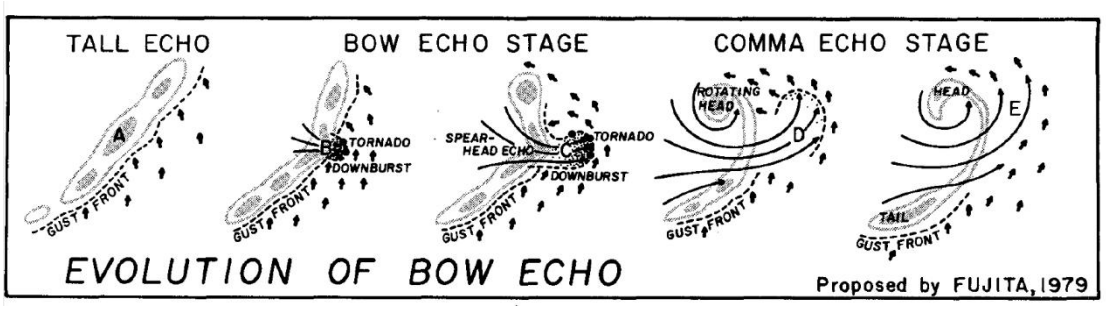

Figure S3. Evolution of bow echo proposed by Fujita. In this model a downburst thunderstorm produces a bow echo. In the comma echo stage (stages D and E), the downburst winds weaken and induces a mesoscale circulation, which distorts the initial line echo into a comma-shaped echo with a rotating head. From Fujita [27].

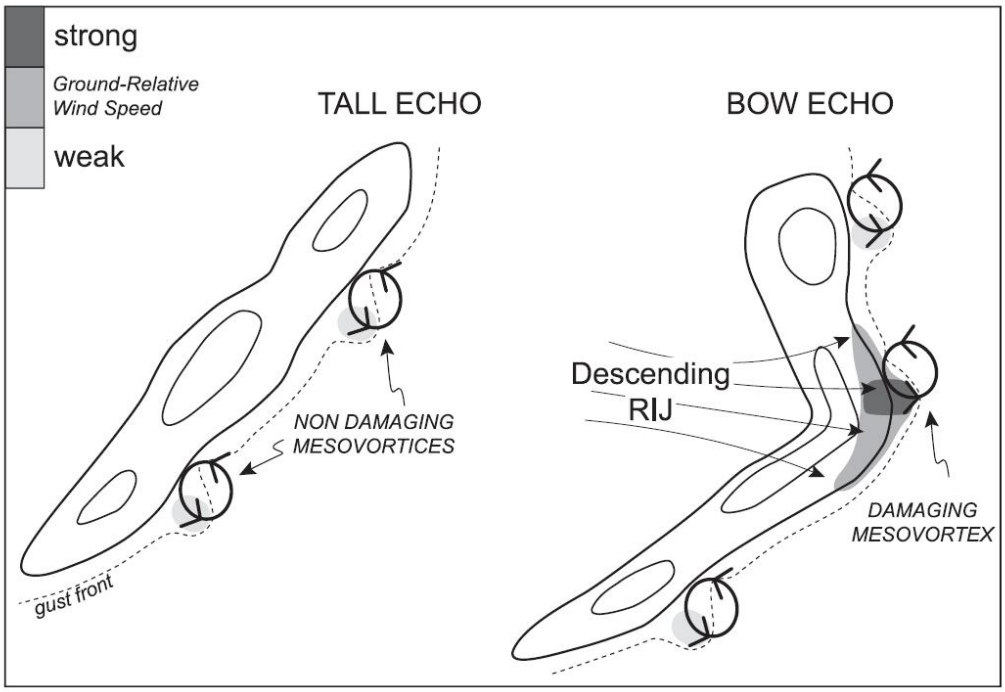

Figure S4. Schematic diagram illustrating damaging and non-damaging mesovortices formed within a bow echo. From Atkins and St. Laurent [36], the dark shading shows where damaging winds are found as a result of the superposition of the RIJ and the mesovortex flow.

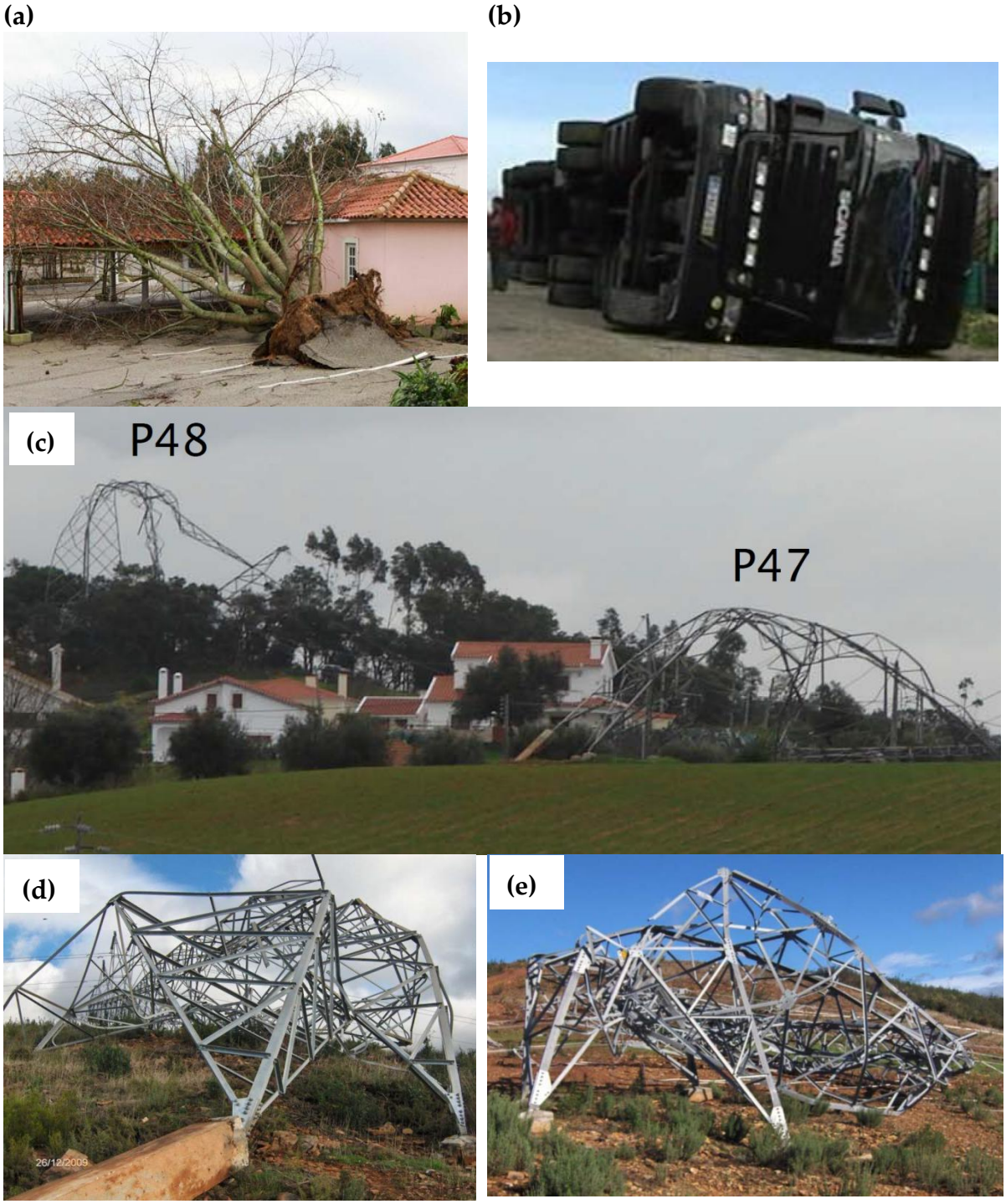

Figure S5. (a)-(d) Damages in the Oeste region. **(a)** Uprooted tree, **(b)** Large vehicle overturned, **(c)** Two power towers (P47, P48) destroyed with houses in between. **(d)** Power tower destroyed including snapped out concrete foundation; **(e)** Power tower destroyed near Portimão (see locations of Oeste region and Portimão in Figure 1d).

48

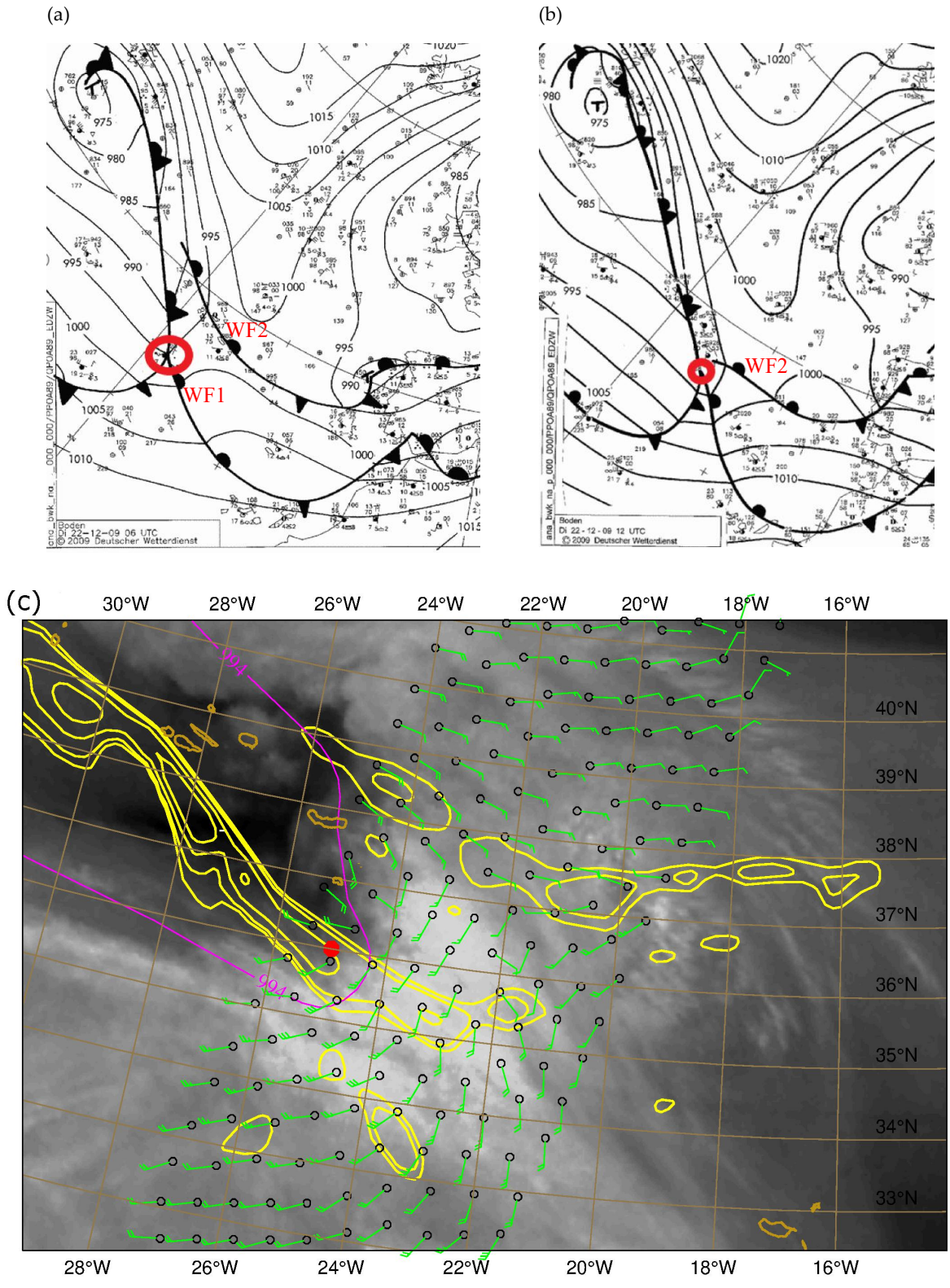

49

50 **Figure S6.** Surface synoptic analysis from Deutscher Wetterdienst **(a)** 0600UTC and **(b)** 1200UTC on
51 22/12/2009. The triple point (i.e., the junction between the occluded, cold, and warm fronts) of an
52 occluded extratropical cyclone is marked by a red circle. The windstorm Xola formed southeast of this
53 triple point, over the warm front, labelled WF1. **(c)** MSG WV6.2 image (at 1115UTC) superimposed with
54 ASCAT winds at 1120UTC and TFP at 925hPa (°C/(100km)^2, yellow lines) at 1200UTC. The MSLP isobar
55 of 994hPa is also shown with a magenta line.

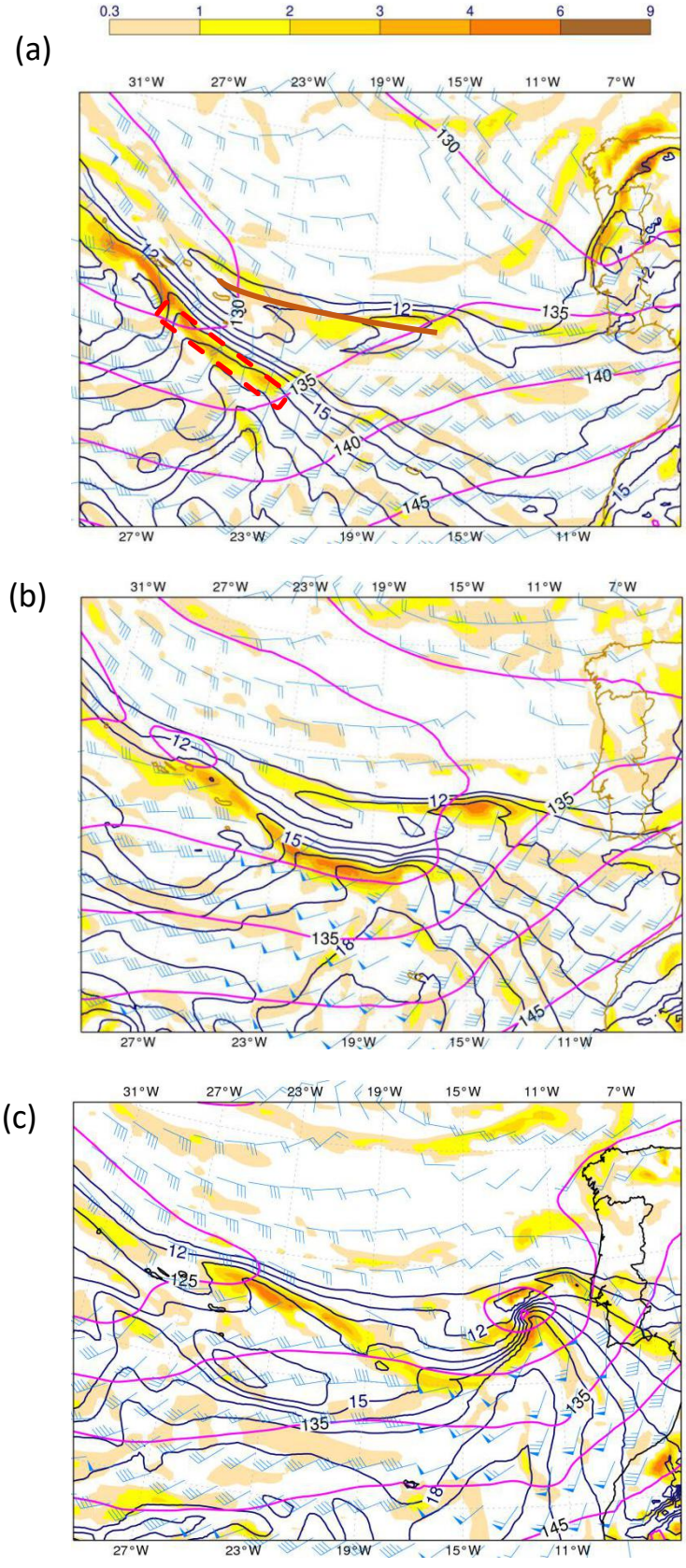

Figure S7. ECMWF analyses valid at **(a)** 1200UTC, **(b)** 1800UTC on 22/12/2009 and **(c)** 0000UTC on 23/12/2009. Wind (blue barbs), TFP (shaded, °C/(100km)^2) and wet-bulb potential temperature (1°C intervals, from 11 to 19°C in black lines) at 925hPa; Geopotential height (5 dam intervals, magenta lines) at 850hPa. In (a) the warm front WF1 is marked with dashed red rectangle and the warm front WF2 is marked with a brown thick line.

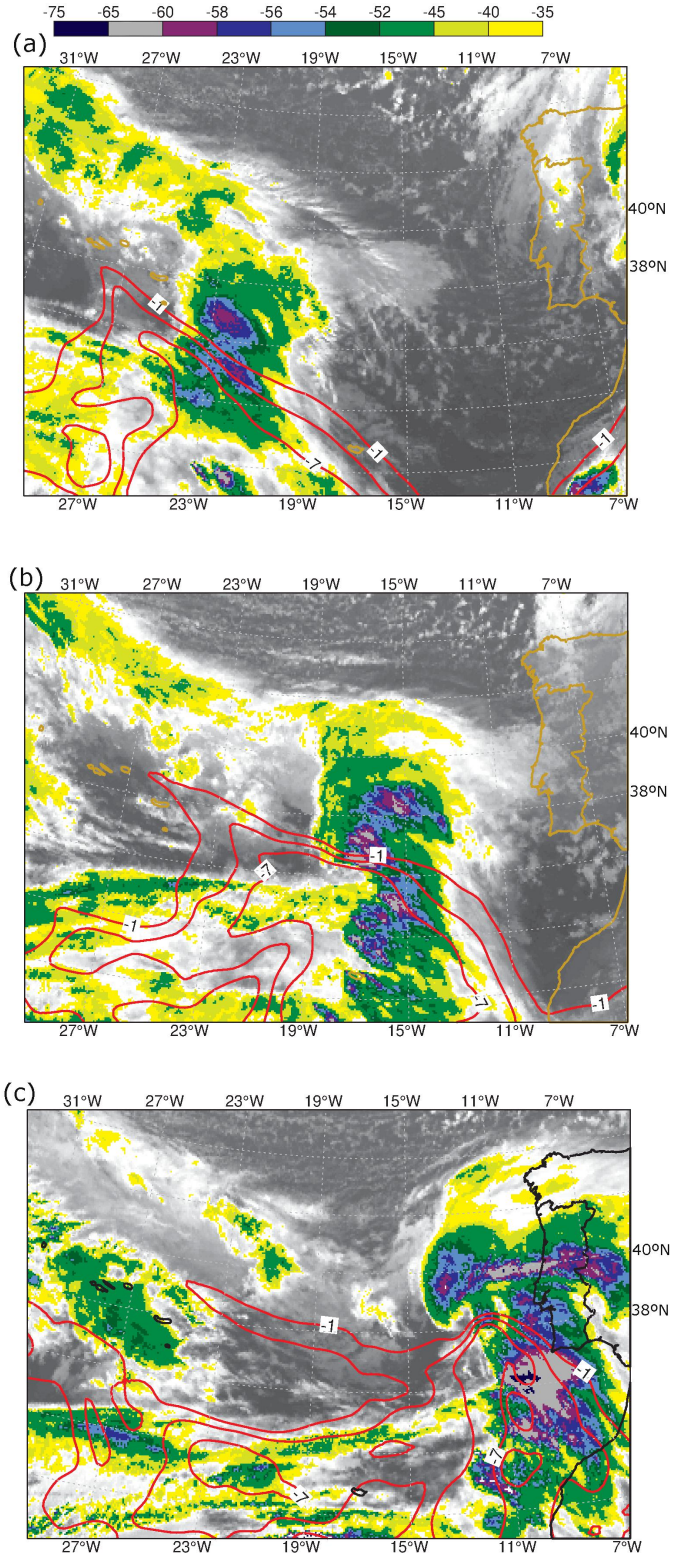

Figure S8. IR10.8 brightness temperature (shaded from -35 to -75°C) superimposed with PI (-1,-4 and -7°C in red lines) for **(a)** 1200UTC, **(b)** 1800UTC on 22/12/2009, and **(c)** 0000UTC on 23/12/2009. See definition of PI in section 2.3.2.

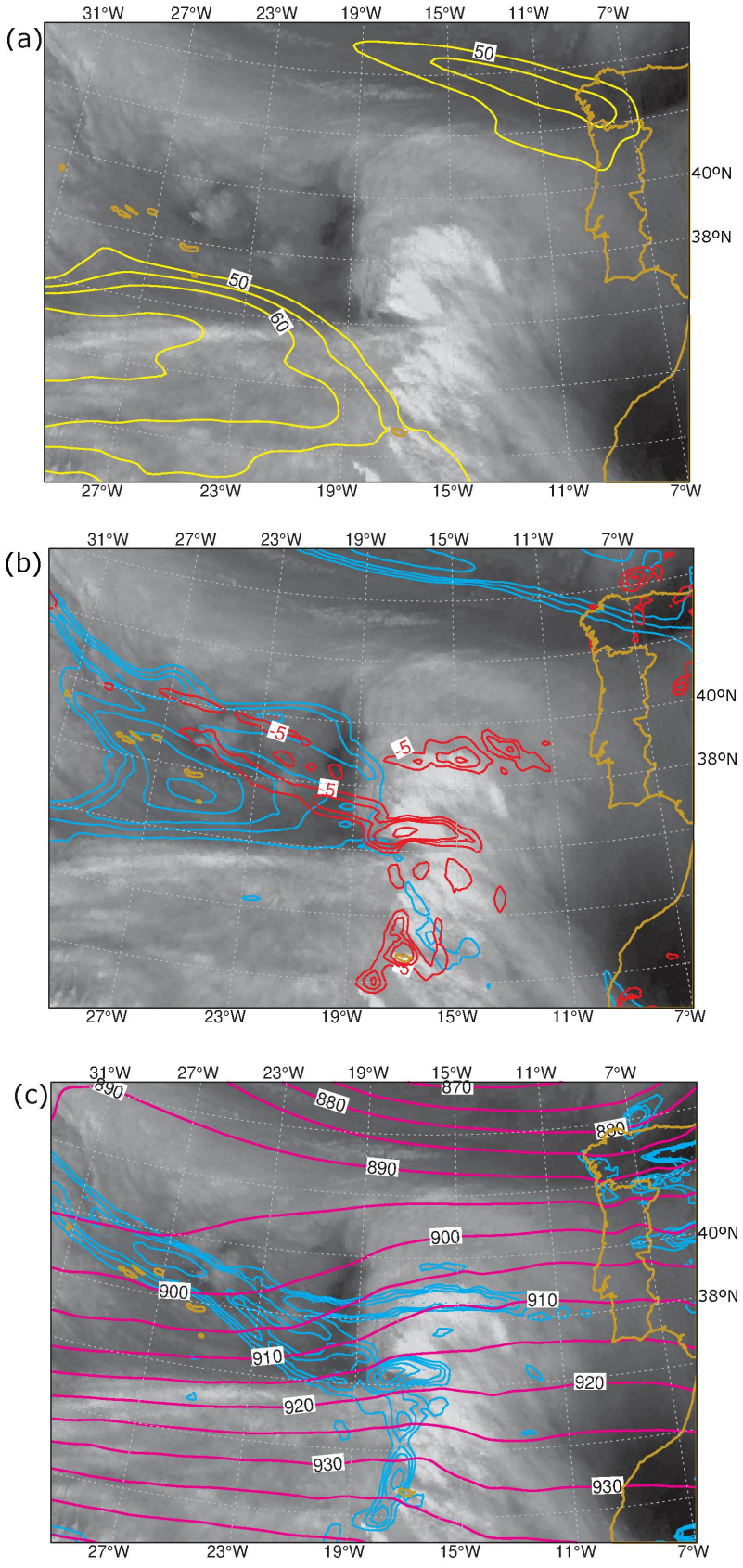

Figure S9. MSG WV6.2 image at 1800UTC on 22/12/2009 superimposed with **(a)** wind speed at 300hPa (50, 55, 60 and 70 m s^{-1}, yellow lines); **(b)** convergence at 850hPa (-5, -10, -15, -30, -50×$10^{-5}s^{-1}$, red lines) and potential vorticity at 300hPa (1, 1.5, 2, 3, 4 PVU, cyan lines), **(c)** Geopotential height at 300hPa (5 dam intervals, blue lines) and relative vorticity at 850hPa (5, 10, 15, 30×$10^{-5}s^{-1}$, blue lines).

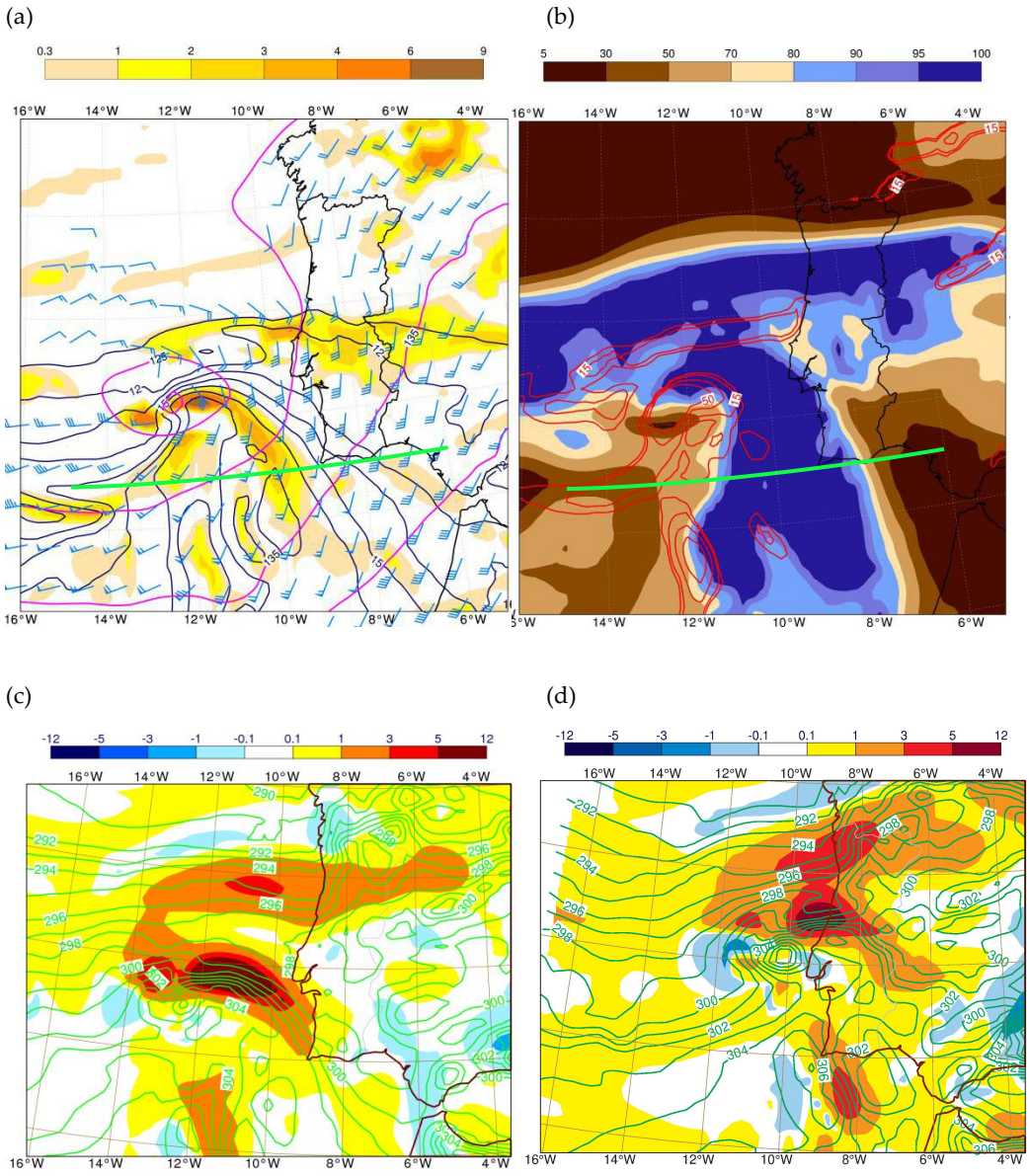

Figure S10. ECMWF analyses at 0000UTC on 23/12/2009. **(a)** Geopotential height (5 dam intervals, magenta lines), wind (blue barbs), θ_w (1°C intervals, from 11 to 18°C in black lines) and TFP (°C/(100km)^2, shaded) at 850hPa. **(b)** Relative humidity (shaded) and relative vorticity (5, 10, 15, 30, 50×10^{-5}s^{-1}, red lines). The green line marks the cross-section that will be represented in Figure S12. Petterssen's Frontogenesis (10^{-9} K m^{-1}s^{-1}, shaded) and potential temperature (1 K intervals, green lines) at 800hPa, at **(c)** 0000UTC (ECMWF analysis) and **(d)** 0300UTC (ECMWF forecast) on 23/12/2009.

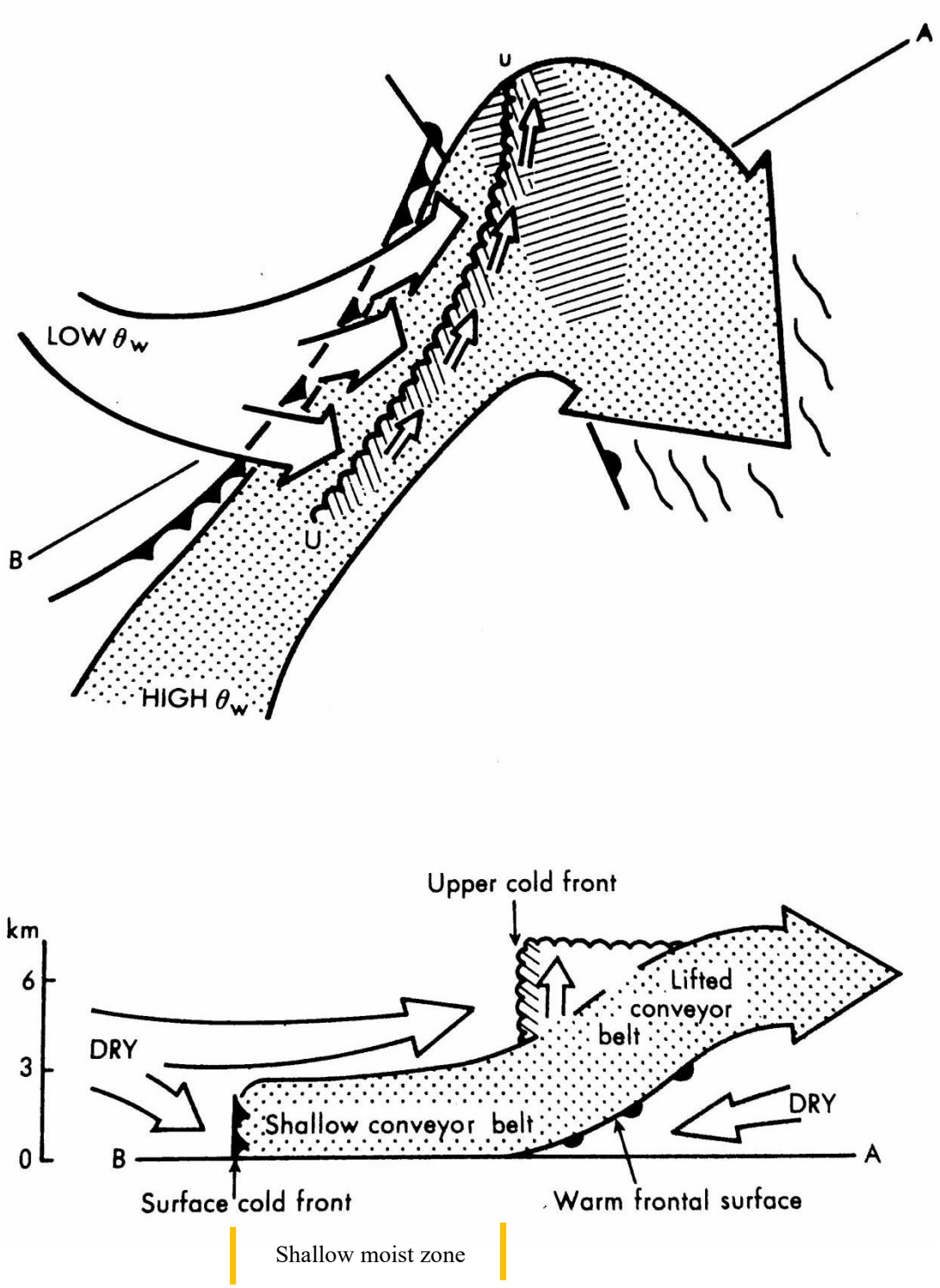

Figure S11. Idealized structure of a kata-cold front, also known as split cold front. (a) Plan view showing that cold and dry air (θw) associated with the dry intrusion overrides moist and warm air in the warm conveyor belt. The line UU represents the upper cold front (b) Vertical cross section along AB. The shallow moist zone is characterized by the presence of low clouds and occurrence of mainly light precipitation. Outbreaks of deep convection are expected in association to the upper cold front. Adapted from Browning and Monk [24].

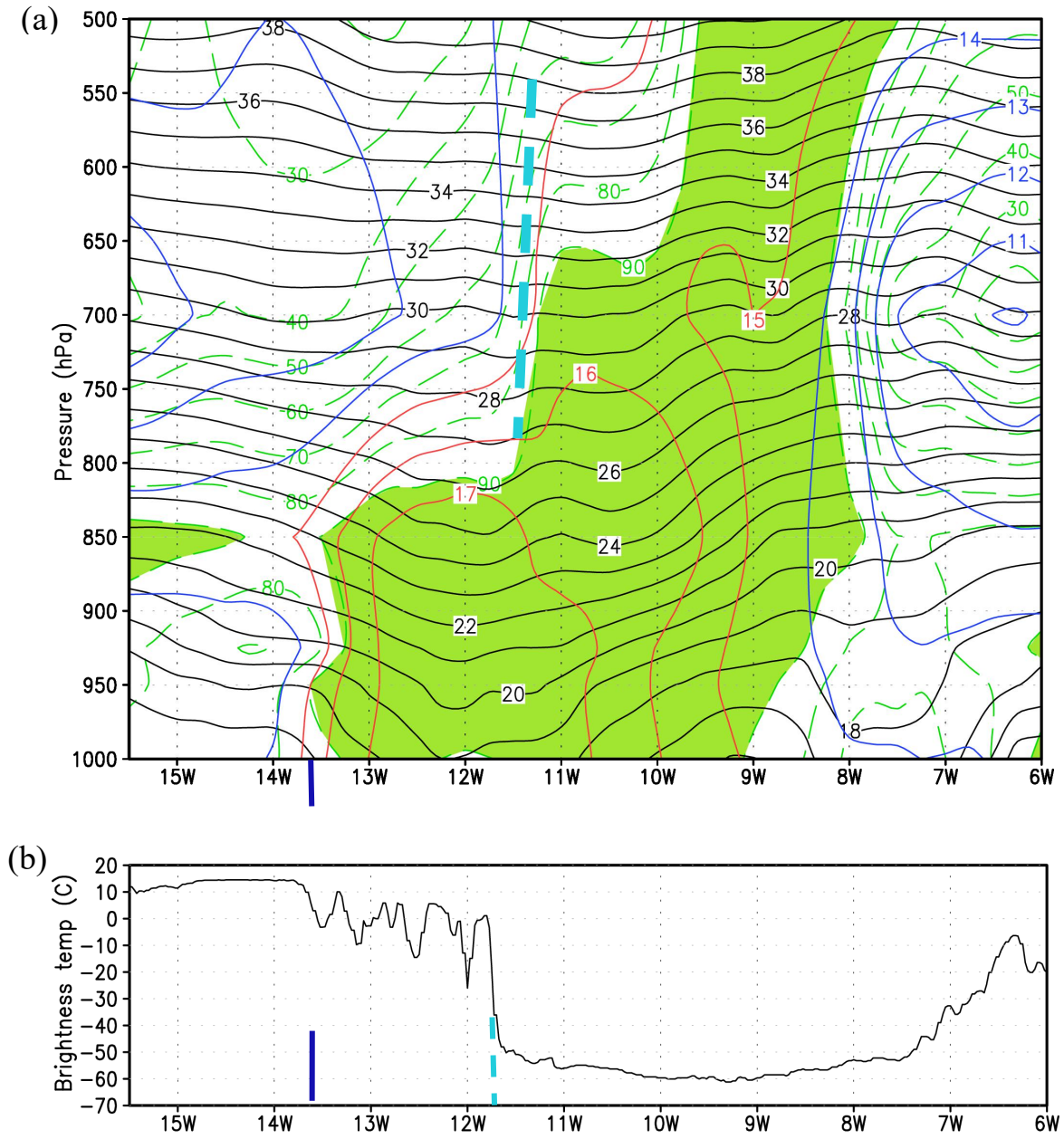

Figure S12. (a) Vertical cross-section along 37°N from 16°W to 6°W (green line marked in Figure S10) of ECMWF analysis fields at 0000UTC on 23/12/2009. Wet-bulb potential temperature (≥ 15°C in red, < 15°C in blue lines) and potential temperature (°C, black solid lines) and relative humidity (green dashed lines from 30 to 90%, green shaded where RH ≥ 90%). **(b)** Cross-section along along 37°N from 16°W to 6°W (green line marked in Figure S10) of IR10.8 brightness temperature (°C, black solid line). The vertical blue and dashed cyan lines indicate the positions of the SCF and UCF, respectively.

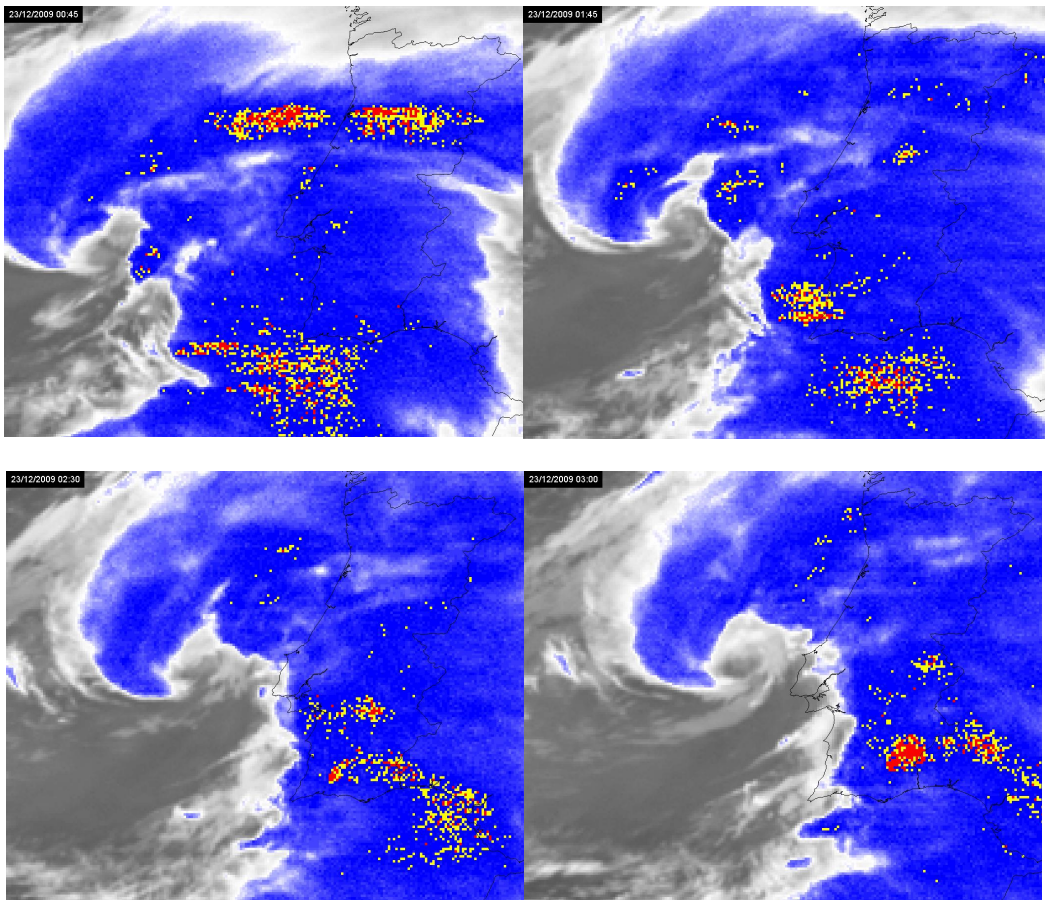

Figure S13. Overshooting top product (WV6.2 and IR10.8 BTD) at 0045UTC, 0145UTC, 0230UTC and 0300UTC on 23/12/2009. The overshooting tops are identified by the yellow and red pixels.

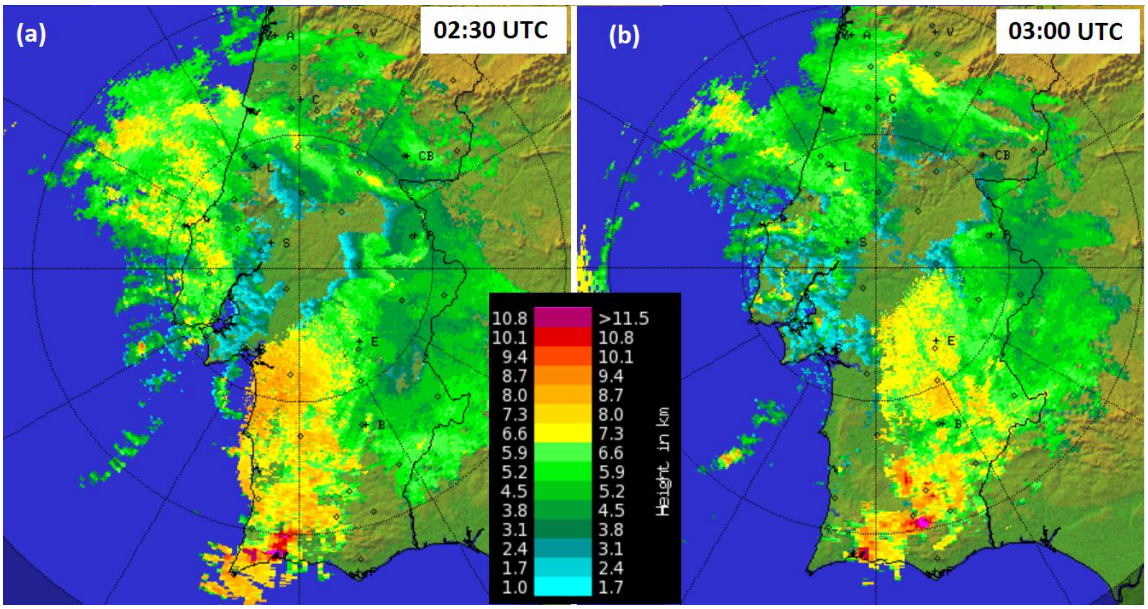

Figure S14. TOPS image from CL radar at (a) 0230 UTC and (b) 0300 UTC on 23/12/2009. Note that the scale is different from that in Figure 11.

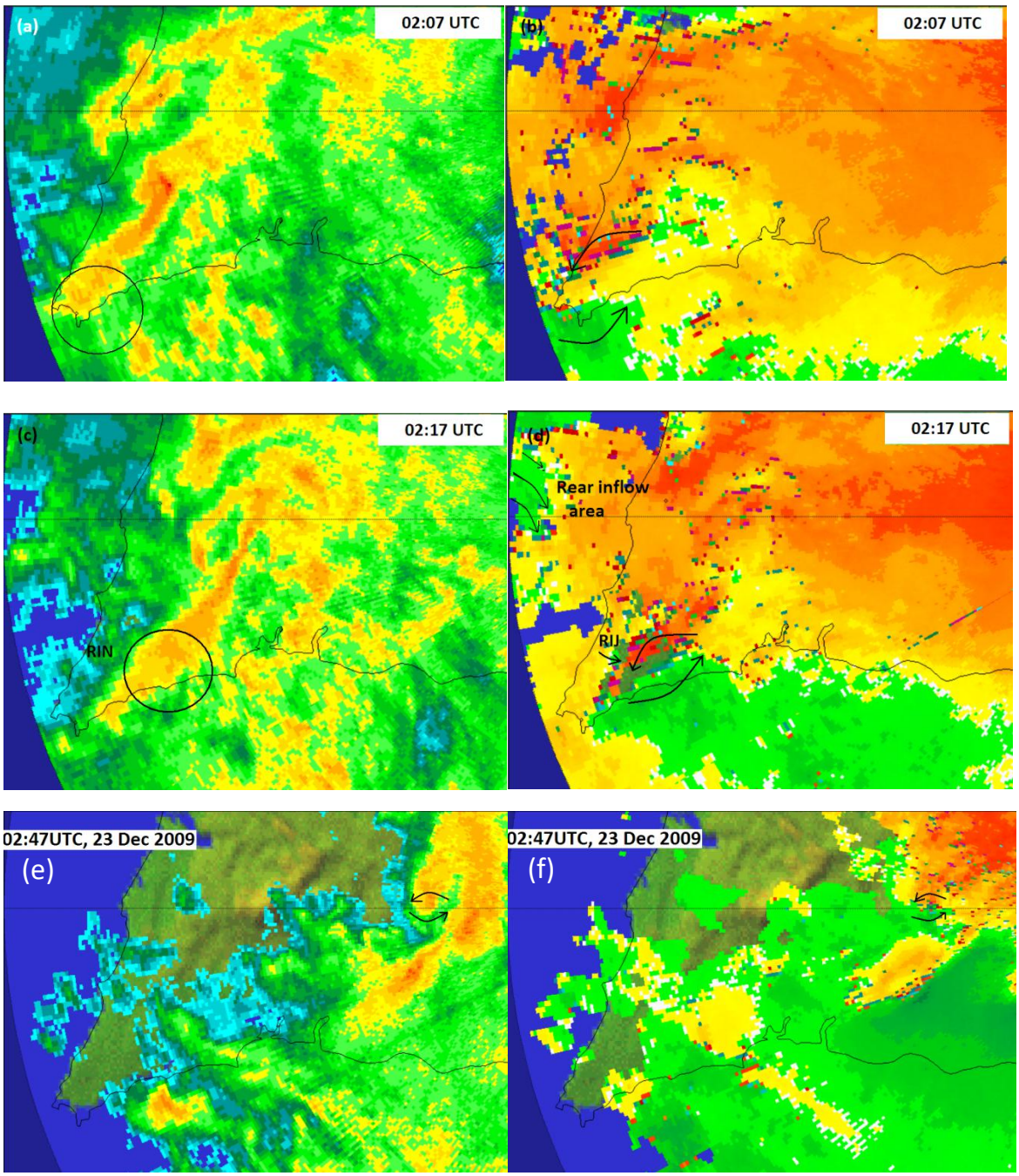

Figure S15. PPI at 1.5° elevation on the 23/12/2009. Radar reflectivity at **(a)** 0217 UTC, **(c)** 0227UTC and **(e)** 0247UTC. Storm-relative velocity at **(b)** 0217 UTC, **(d)** 0227UTC and **(f)** 0247UTC. Bow echo is marked with oval and RIN signature are marked in (a, c); black circular arrows represent the approximate circulation of the mesovortex and RIJ signature is marked when identified (b, d). Rear inflow area marked with black arrows in (d). The average storm translation vector in the period 0200-0250 UTC was 36 ms^{-1} from 234°. The scales are the same as in Figure 8.

Table S1. InV and OutV are the maximum inbound (approaching the radar) and outbound storm-relative velocities. V-diam is couplet diameter, defined by the distance between the pixels of InV and OutV. Az Shear is the azimuthal shear, defined as the difference between OutV and InV normalized by V-diam. M-RotV is the maximum rotational velocity (average magnitude of inbound and outbound velocities). Alt is the altitude at which the rotation couplet is observed. Range is the distance between the couplet and the radar.

Time (UTC) (tilt ^{0})	InV (m/s)	OutV (m/s)	V-diam (km)	Az Shear (x10^{-3} s^{-1})	M-RotV (m/s)	Alt (km)	Range (km)
0207 (1.5)	-9.45	+24.8	11.3	3.0	17.2	3.5	91
0217 (1.5)	-10.04	+30.1	11.2	3.6	20.0	3.0	78
0227 (0.1)	-5.91	+20.67	3.4	7.8	13.3	1.0	63
0227 (1.5)	-8.27	+27.76	4.6	7.8	18.0	2.5	63
0227 (4.0)	-13.58	+17.13	8.4	3.7	15.4	5.3	63
0237 (0.1)	-25.98	+23.0	1.6	30.6	24.5	0.8	48
0237 (1.5)	-16.54	21.26	5.0	7.6	18.9	2.0	48
0237 (4.0)	-21.85	+14.17	1.5	24.0	18.0	4.0	48
0247 (0.1)	-11.81	+23.6	2.4	14.8	17.7	0.7	33
0247 (1.5)	-10.6	+20.08	2.4	13.1	15.3	1.6	33
0247 (4.0)	-12.4	+10.04	2.4	9.4	11.2	3.0	33

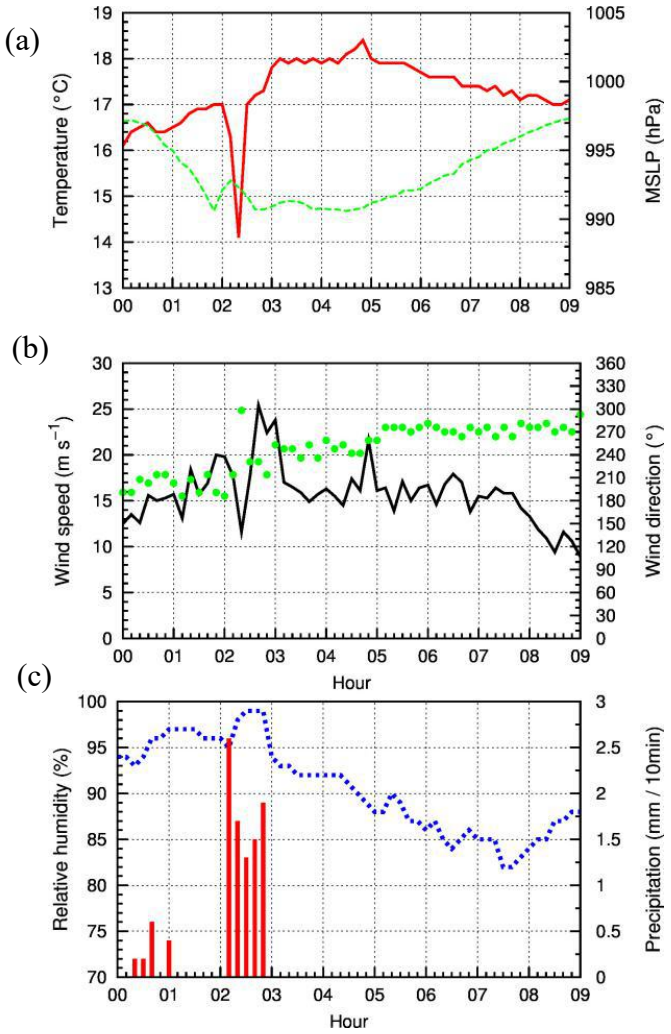

Figure S16. Time evolution of (a) 2 m temperature (red line) and MSLP, (b) wind gust (black line) and wind direction at 10 m and (c) relative humidity (blue dashed line) and 10 minutes accumulated precipitation at Sagres station, on 23/12/2009 (see its location in Figure 1d).

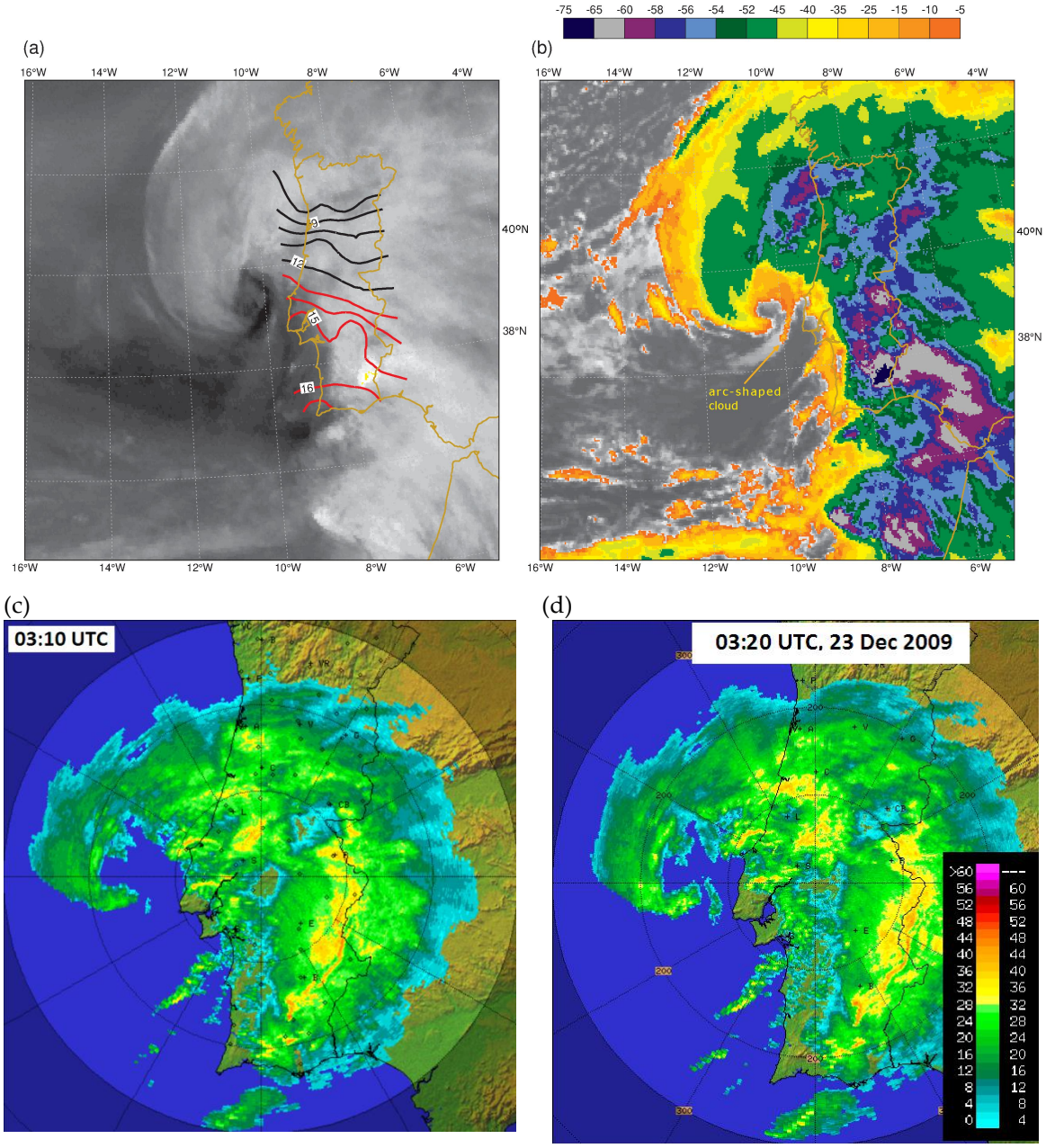

139 **Figure S17.** (a) MSG WV6.2 image and (b) IR10.8 brightness temperature (shaded from -5 to -70°C) at 0310UTC
140 on 23/12/2009. MAXZ from CL radar at (c) 0310UTC and (d) 0320UTC on 23/12/2009.

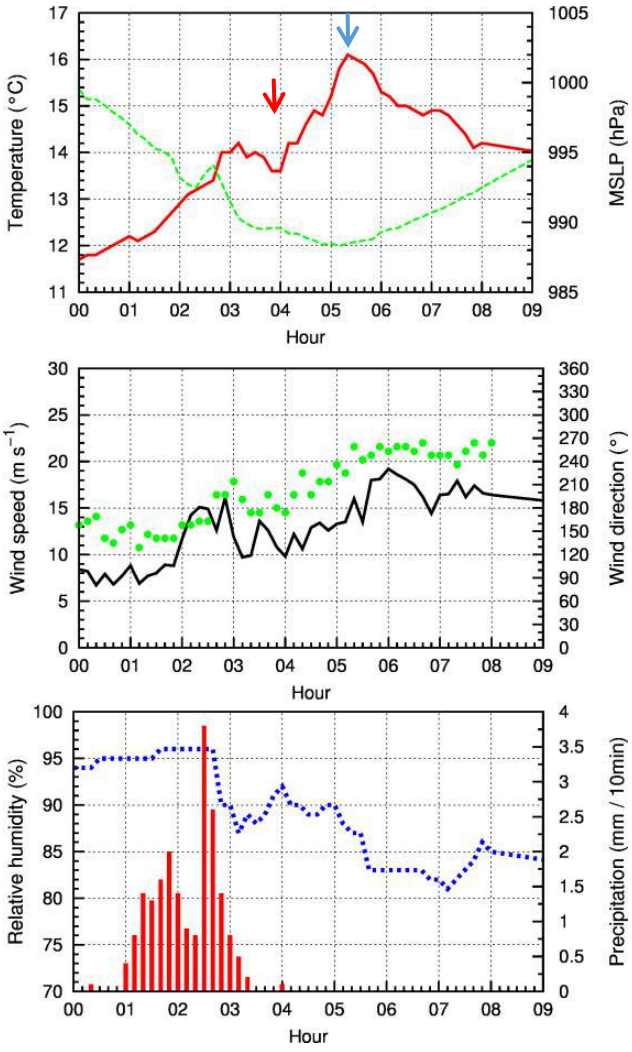

Figure S18. Same as in Figure S16 but for Beja station (see its location in Figure 1d).

155

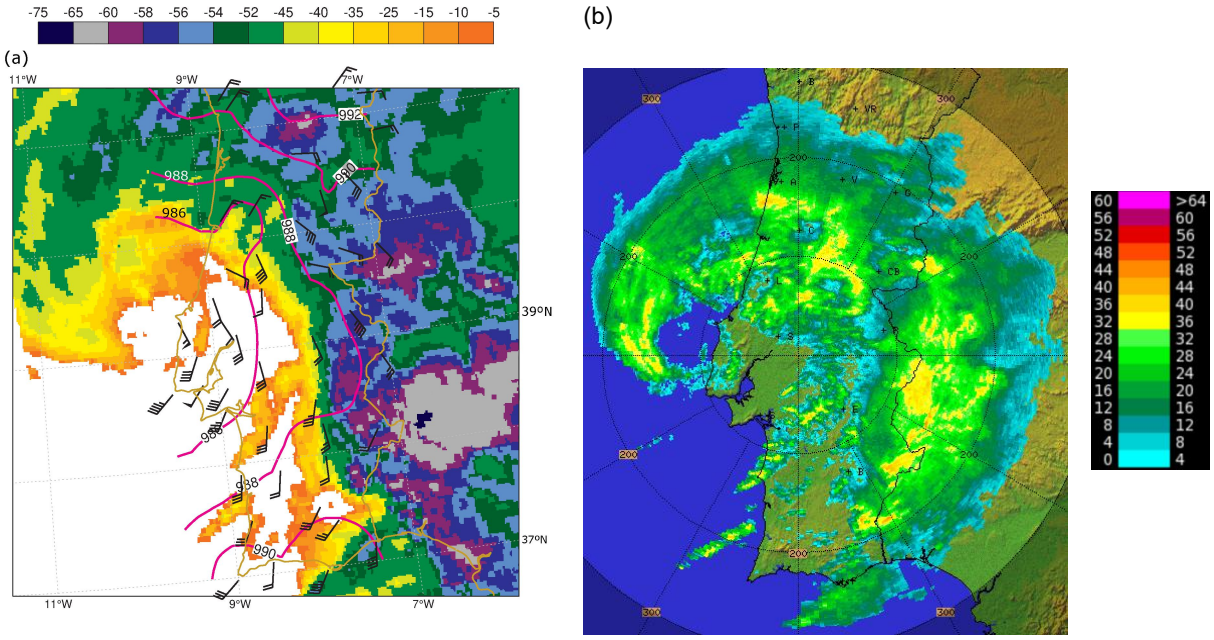

156 **Figure S19 (a)** IR10.8 brightness temperature (shaded from -5 to -75°C) superimposed with observations of
157 MSLP (2hPa intervals, magenta lines) and wind gust at 10 m (barbs) at 0350UTC. **(b)** MAXZ from CL radar at
158 0350UTC on 23/12/2009.

159

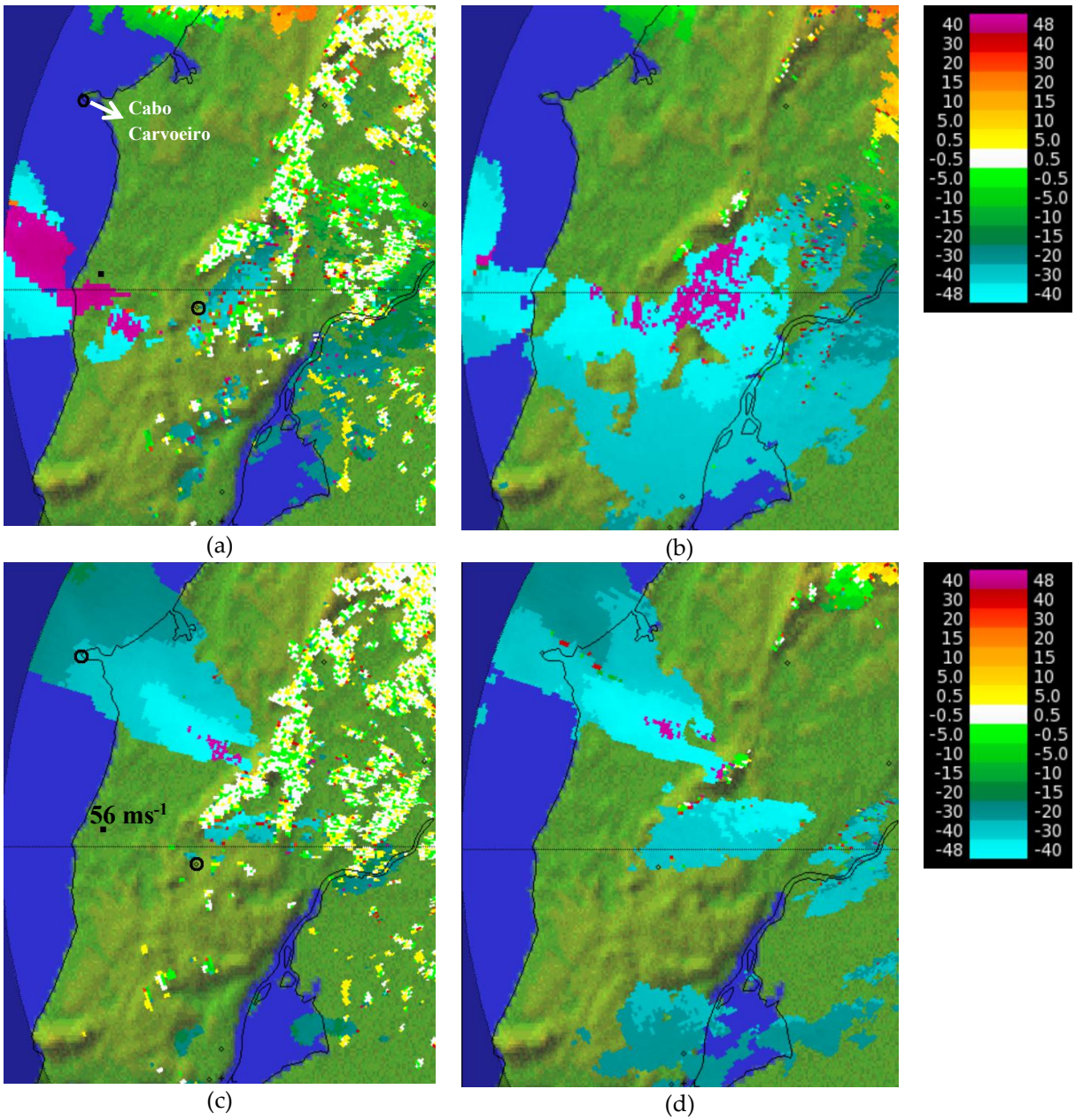

Figure S20. Doppler velocity (PPI at 0.1⁰ elevation) at (a) 0426 UTC and (c) 0446 UTC, showing the jet streak at an altitude of 500-950 m. Doppler velocity (PPI at 1.5⁰ elevation) at (b) 0427 UTC and (d) 0447 UTC, showing the jet streak at an altitude of 1400-2500 m, on the 23/12/2009.

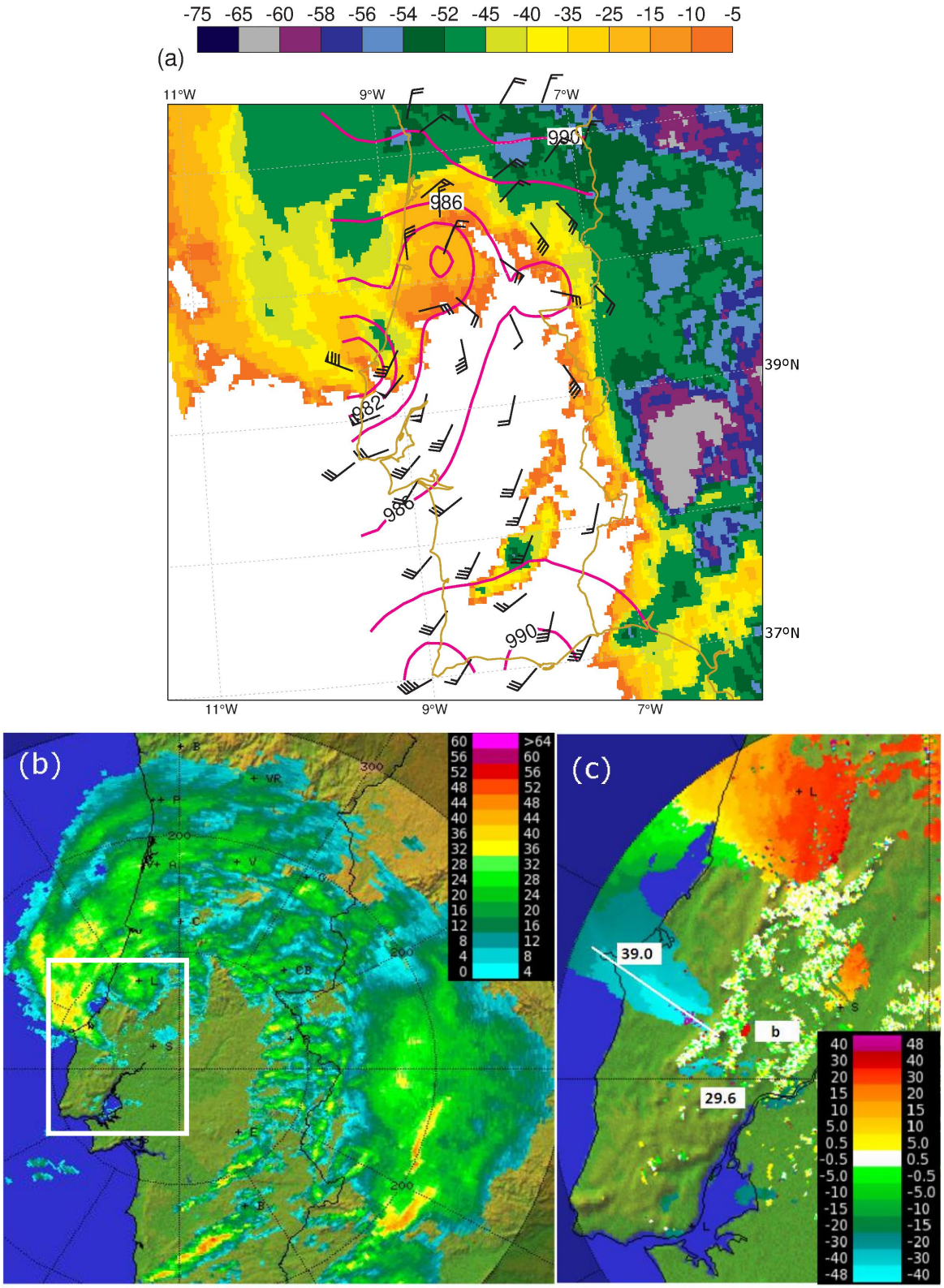

Figure S21. Observations at 0450UTC on 23/12/2009. **(a)** IR10.8 brightness temperature (shaded from -5 to -75°C) superimposed with observations of MSLP (2hPa intervals, magenta lines) and wind gust at 10 m (barbs) at 0450UTC. **(b)** MAXZ from CL radar. **(c)** Doppler velocity (PPI at 0.1º elevation) at 0446 UTC, showing the jet streak at an altitude of 500-950 m. Indicated wind gusts at the time in the represented locations. The approximate location where power towers where completely destroyed is marked with "b".

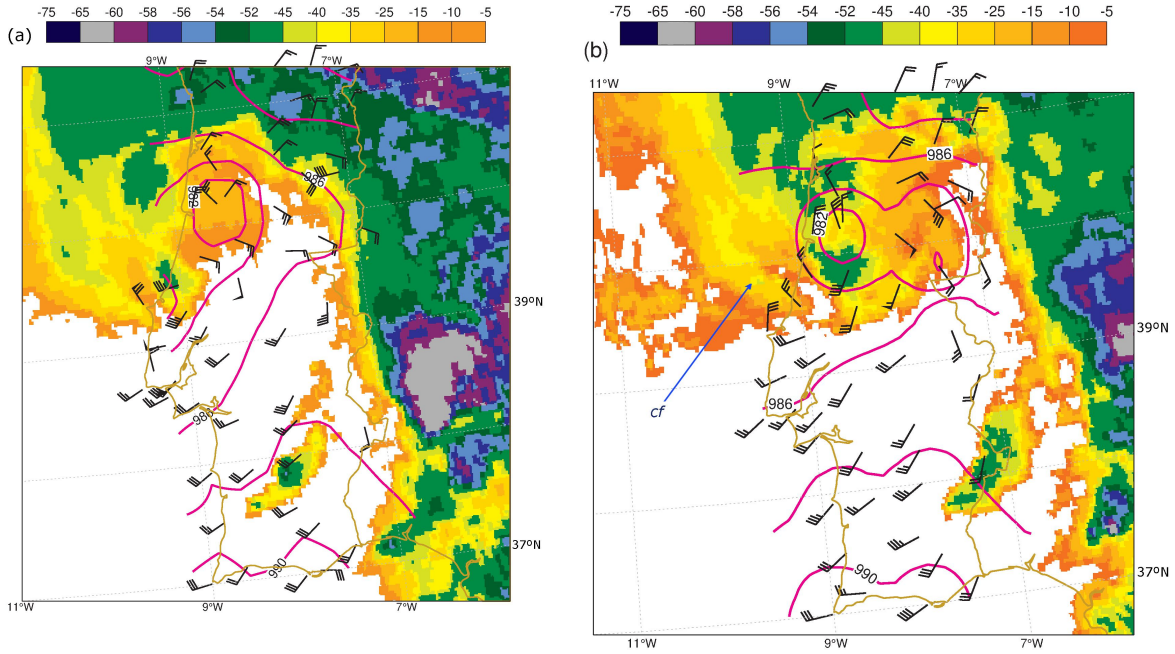

Figure S22. IR10.8 brightness temperature (shaded from -5 to -75°C) superimposed with observations of MSLP (2hPa intervals, magenta lines) and wind gust at 10 m (barbs) at **(a)** 0500UTC and **(b)** 0540UTC on 23/12/2009. The dissipating cloud filament (labelled as *cf*) is marked in (b).